A cohesive-zone crack healing model for self-healing materials

Ponnusami, Sathiskumar A.; Krishnasamy, Jayaprakash; Turteltaub, Sergio; van der Zwaag, Sybrand

DOI
10.1016/j.ijsolstr.2017.11.004

Publication date
2018

Document Version
Final published version

Published in
International Journal of Solids and Structures

International Journal of Solids and Structures 134 (2018) 249–263

Contents lists available at ScienceDirect

International Journal of Solids and Structures

journal homepage: www.elsevier.com/locate/ijsolstr

A cohesive-zone crack healing model for self-healing materials

Sathiskumar A. Ponnusami[1], Jayaprakash Krishnasamy, Sergio Turteltaub*, Sybrand van der Zwaag

Faculty of Aerospace Engineering, Delft University of Technology, Kluyverweg 1, Delft 2629 HS, The Netherlands

ARTICLE INFO

Article history:
Received 7 July 2017
Revised 28 September 2017
Available online 7 November 2017

Keywords:
Self-healing material
Cohesive-zone model
Multiple crack healing
Fracture mechanics

ABSTRACT

A cohesive zone-based constitutive model, originally developed to model fracture, is extended to include a healing variable to simulate crack healing processes and thus recovery of mechanical properties. The proposed cohesive relation is a composite-type material model that accounts for the properties of both the original and the healing material, which are typically different. The constitutive model is designed to capture multiple healing events, which is relevant for self-healing materials that are capable of generating repeated healing. The model can be implemented in a finite element framework through the use of cohesive elements or the extended finite element method (XFEM). The resulting numerical framework is capable of modeling both extrinsic and intrinsic self-healing materials. Salient features of the model are demonstrated through various homogeneous deformations and healing processes followed by applications of the model to a self-healing material system based on embedded healing particles under non-homogeneous deformations. It is shown that the model is suitable for analyzing and optimizing existing self-healing materials or for designing new self-healing materials with improved lifetime characteristics based on multiple healing events.

1. Introduction

The concept of self-healing is a promising path to enhance the damage tolerance and extend the lifetime of structural and functional materials. Research in the last decade has shown that self-healing mechanisms can be incorporated in various material classes ranging from polymers to high temperature ceramics (van der Zwaag, 2008). A classical example of an *extrinsic* self-healing mechanism is based on healing capsules (particles) dispersed within the base (or matrix) material as shown in Fig. 1a. In an extrinsic system, the healing process is typically activated by cracks that interact with the capsules (White et al., 2001; Kessler et al., 2003; Carabat et al., 2015). Such capsule-based self-healing mechanism finds its application in materials that otherwise do not possess the capacity to repair damage. Other extrinsic self-healing materials involve hollow fibers filled with healing agents (Pang and Bond, 2005a; Dry, 1994) and microvascular networks with distributed healing agents (Toohey et al., 2007). Among the extrinsic self-healing mechanisms, the encapsulated particle-based system has been widely investigated (Blaiszik et al., 2010; Wiktor and Jonkers, 2011; Van Tittelboom and De Belie, 2013). The encapsulation-based healing concept may lead to a desirable autonomous self-healing behavior for the system (base material plus healing agent), but it is typically limited by the finite amount of the healing agent which often precludes multiple healing, at least in the location where the healing agent has been consumed. Microvascular network-based self-healing systems offer the possibility of multiple healing after repeated damage events by enhancing the supply of the healing agent. In contrast with extrinsic self-healing material systems, in *intrinsic* self-healing materials the healing action is due to the physio-chemical nature of the material itself, as illustrated in Fig. 1b (Bergman and Wudl, 2008). Such materials have the natural capability of repairing the damage more than once (Sloof et al., 2016).

Though extensive research has been conducted in realizing such material systems experimentally, efforts to develop computational models that could simulate fracture and healing have been scarce. Simulation-based design guidelines can be used to optimize self-healing systems. Consequently, the goal of the present work is to develop a computational framework to model the effect of crack healing behavior on the mechanical performance of the material or the structure under consideration. The modeling and computa-

* Corresponding author.
E-mail addresses: S.AnusuyaPonnusami@tudelft.nl, sathis.ponnusami@eng.ox.ac.uk (S.A. Ponnusami), J.Krishnasamy-1@tudelft.nl (J. Krishnasamy), S.R.Turteltaub@tudelft.nl (S. Turteltaub), S.vanderZwaag@tudelft.nl (S. van der Zwaag).
[1] Current address: Solid Mechanics and Materials Engineering, Department of Engineering Science, University of Oxford, Parks Road, OX1 3PJ Oxford, United Kingdom.

https://doi.org/10.1016/j.ijsolstr.2017.11.004
0020-7683/

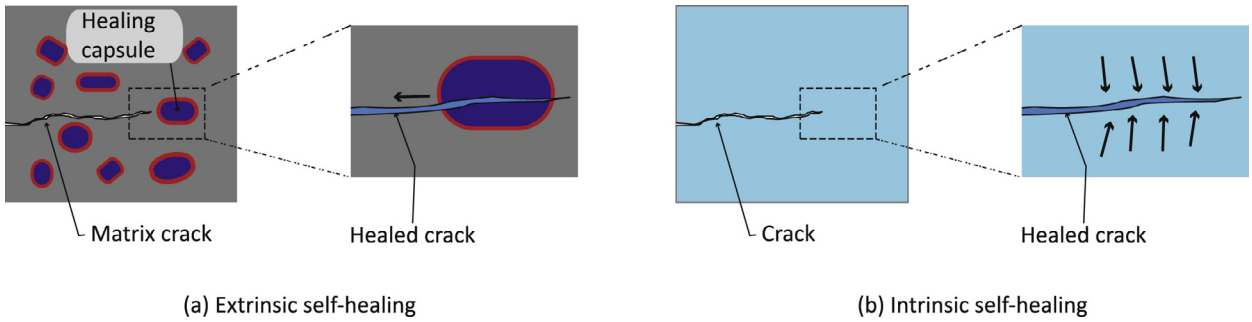

Fig. 1. Schematic of (a) a capsule-based extrinsic self-healing material: a matrix crack is attracted towards the healing capsule, which upon fracture releases the healing agent into the crack, resulting in crack healing and (b) an intrinsic self-healing material: the healing agent is available directly from the material chemical composition. The material that fills the crack is typically different than the matrix material for both the extrinsic and intrinsic cases.

tional framework is kept sufficiently general such that it is capable of analyzing both extrinsic and intrinsic self-healing materials.

In the context of a capsule (or fiber)-based extrinsic self-healing system, there are two critical aspects that need to be addressed in order to achieve a robust self-healing system. Firstly, a crack initiated in the host (or matrix) material should be attracted towards the healing particle (or fiber) and further should break the particle for healing to occur. A schematic of such self-healing material and the associated healing mechanism is shown in Fig. 1. Crack-particle interaction, which is a crucial aspect to successfully trigger the healing mechanism, has been analyzed parametrically in Ponnusami et al. (2015a, 2015b) to generate design guidelines for the selection of the healing particles in terms of their mechanical properties. Other studies in the literature have utilized analytical and numerical techniques to investigate the interaction between the crack and the healing particles or capsules (Zemskov et al., 2011; Gilabert et al., 2017; Šavija et al., 2016). The second critical aspect in a self-healing system, relevant for both extrinsic and intrinsic mechanisms, is centered on how the material recovers its mechanical properties once the healing mechanism is activated in or near the fracture surfaces. In particular, the recovery of load-carrying capability as a function of healing parameters, crack length and capsule properties is a subject of importance but has not received adequate attention in the literature yet. Consequently, one main focus of the current research is to simulate the recovery of mechanical properties of the self-healing system.

Research efforts have been made in the literature to model the mechanical behavior of materials taking both fracture and healing into account. Most of the existing models adopt a continuum damage mechanics-based approach whereby cracking and healing are interpreted as a degradation or recovery of material stiffness and strength (Barbero et al., 2005; Voyiadjis et al., 2011; 2012; Mergheim and Steinmann, 2013; Darabi et al., 2012; Xu et al., 2014; Ozaki et al., 2016). The common feature of these models is that the internal variables describing the continuum degradation and healing of the material refer to the effective behavior of (unresolved) cracking and healing events. Correspondingly, details at the level of individual cracks are not explicitly taken into account. However, a direct description at the level of individual cracks and healing particles is desirable in view of designing or fine-tuning a self-healing material.

Cohesive zone-based approaches have also been proposed for modeling crack healing. Unlike continuum damage models, the advantage of the above cohesive zone approaches is that the material damage is treated in a discrete manner as cohesive cracks, which allows for explicit modeling of crack evolution and its healing. In Maiti and Geubelle (2006), crack healing is simulated through an artificial crack closure technique by introducing a wedge into the crack. The methodology is implemented in a finite element framework using cohesive elements for simulating fracture and a contact law that enforces the conditions for crack healing or retardation. In Schimmel and Remmers (2006) a Mode I exponential cohesive zone model is proposed to simulate crack healing by introducing a jump in crack opening displacement. After model verification, they applied the framework to simulate delamination crack healing in a slender beam specimen to show the capability of the model. Some limitations of the model are with regard to the multiple healing events and their one-dimensionality. In Ural et al. (2009), a cohesive zone model for fatigue crack growth is developed, which also considers crack retardation during unloading regimes. In Alsheghri and Al-Rub (2015) a thermodynamics-based cohesive zone methodology is used to model crack healing behavior by extending previous work on continuum damage-healing mechanics (Darabi et al., 2012). The model takes into account the effect of various parameters such as temperature, resting time and crack closure on the healing behavior. However, the fracture properties of the healed zone, upon complete healing, assume the values of the original material, which is often not the case even for intrinsic self-healing materials. Furthermore, the capability of simulating multiple healing events is not demonstrated in many of the above-mentioned studies, which is of direct relevance for intrinsic self-healing materials or extrinsic systems with a continuous supply of healing agent. Other modeling approaches explored in the literature to simulate crack healing behavior are based on the theory of porous media (Bluhm et al., 2015) or the discrete element method (Luding and Suiker, 2008; Herbst and Luding, 2008).

To overcome the limitations in the existing models in the literature, a generalized cohesive-zone based crack healing model is developed here, which can be applied to both extrinsic and intrinsic self-healing materials. The model is capable of simulating property recovery after multiple healing events and is also able to handle different fracture properties for the healing material as compared to that of the original material. An additional feature of the model is that the properties of the healing material may be specified separately for different healing instances. This is particularly important as the recovery of the fracture properties in the healed zone is not always complete, resulting in varying fracture properties for each healing instance that depend, among others, on healing time, diffusion-reaction characteristics and temperature. It is noted that the model developed here does not explicitly aim to capture the actual healing kinetics, but to simulate the recovery of the overall load bearing capacity as a function of crack filling and fracture properties of the filling material. Nonetheless, detailed healing kinetics of a material can be coupled to the present model through fracture properties and crack filling behavior to simulate specific materials.

The paper is organized as follows: the proposed crack healing model based on a cohesive zone approach and its finite element

implementation are described in detail in Section 2. Verification of the model is done through basic tests in Section 3, from which salient features of the model are demonstrated. Section 4 is devoted to the application of the model to a particle-based extrinsic self-healing system under mechanical loading. Parametric studies are conducted to showcase the applicability of the model considering some realistic scenarios and the results are reported. Concluding remarks and further work are highlighted in Section 5.

2. Modeling of fracture and healing

A cohesive zone-based fracture mechanics model is extended to model both the fracture and the healing in a unified constitutive relation. In the current fracture-healing framework, the following modeling considerations are made. Firstly, the crack healing model does not include healing kinetics explicitly, rather the focus is to develop a methodology to simulate cracking and the recovery of mechanical integrity upon healing. Consequently, whenever the healing process is activated at a location within the cohesive crack, the resting period is assumed to be sufficiently long such that complete healing occurs. This assumption is not necessary *per se*, but enforced in order to have a specific focus on recovery of mechanical properties using a modified cohesive constitutive relation. Nonetheless, depending upon the type of healing process involved in a specific healing material system, appropriate healing kinetics can be treated separately and coupled with the present framework. This, in turn, can govern the effect of parameters such as resting time and temperature on the degree of healing, which can then be fed as an input to the present framework through appropriately defined fracture properties of the healed material phases. This aspect of healing kinetics is the subject of companion work by the authors and their collaborators.

In the following subsection, the cohesive crack model without healing is discussed first, which is then followed by a discussion on the cohesive crack healing model. The numerical implementation is addressed in the last sub-section.

2.1. Cohesive crack model without healing

The cohesive zone model employed in this work corresponds to a bilinear relation given by T, which is a scalar measure of the traction $\boldsymbol{t}$ transmitted across the cohesive surface, as a function of Δ, which is a scalar measure of the cohesive surface opening displacement vector $\boldsymbol{\delta}$. Though several other cohesive relations have been proposed in the literature, a bilinear relation captures the essential ingredients of most cohesive relations, namely the cohesive strength σ_c and the fracture energy G_c, which are viewed as variable material properties in the present healing model. The traction T increases with increasing cohesive surface opening displacement Δ up to a maximum value given by the strength, σ_c, and eventually decreases to zero, at which point the cohesive zone is fully-separated in the sense that no (positive) traction can be transmitted across the surface. The initial (increasing) part of the cohesive response is useful in conjunction with cohesive elements but may be omitted for XFEM implementations where the cohesive relation is only activated when the critical value σ_c is reached. The area under the traction–separation curve, which represents the total work per unit area expended in creating a fully-separated crack, corresponds to the fracture energy G_c of the material.

An effective crack opening displacement variable is introduced as follows:

$$\Delta := \sqrt{\langle \delta_n \rangle^2 + \gamma^2 (\delta_s)^2}\,, \tag{1}$$

where δ_n and δ_s are, respectively, the normal and tangential components of the crack opening displacement vector $\boldsymbol{\delta}$ resolved in a coordinate system aligned with the local normal and tangential directions of a crack surface. In (1), $\langle\cdot\rangle := (\cdot + |\cdot|)/2$ refers to the Macaulay bracket and γ is a non-dimensional weighting factor for the normal and tangential contributions given by

$$\gamma := \frac{\delta_{n,0}}{\delta_{s,0}}\,,$$

where $\delta_{n,0}$ and $\delta_{s,0}$ denote, respectively, the crack opening at the onset of failure for a pure normal and a pure tangential opening with respect to the crack surface.

In order to determine whether the crack opening is increasing or decreasing due to the external loading process, the following loading function f is used:

$$f = \hat{f}(\Delta, \kappa) := \Delta - \kappa\,, \tag{2}$$

where κ is a damage history variable that, at a given time t, corresponds to the maximum value attained by the equivalent crack opening during a process up to that time, i.e.,

$$\kappa(t) := \max_{\tilde{t}\in[0,t]} \Delta\left(\tilde{t}\right)\,.$$

The Karush–Kuhn–Tucker relations for the loading and unloading conditions can be expressed as follows:

$$f\dot{\kappa} = 0\,, \qquad f \le 0\,, \qquad \dot{\kappa} \ge 0\,, \tag{3}$$

where $\dot{\kappa}$ indicates the (time) rate of change of the damage history variable with $\dot{\kappa} > 0$ corresponding to an active damage step and $\dot{\kappa} = 0$ to an "elastic" step.

The equivalent crack opening is used to compute the equivalent traction T as

$$T = \hat{T}(\Delta, \kappa) = \begin{cases} \hat{g}(\Delta) & \text{if} \quad f = 0 \text{ and } \dot{\kappa} > 0, \\ \hat{g}(\kappa)\dfrac{\Delta}{\kappa} & \text{otherwise}, \end{cases} \tag{4}$$

where $\hat{g}$ is the effective traction–separation law. The upper and lower expressions in (4) provide the equivalent traction during, respectively, crack growth and unloading/reloading.

The specific form of the effective traction–separation law used in the present work is a linear softening relation, which corresponds to

$$g = \hat{g}(\Delta) = \sigma_c \frac{\langle \Delta_f - \Delta \rangle}{\Delta_f - \Delta_i}\,. \tag{5}$$

In the above expression, the parameters Δ_i and Δ_f are, respectively, the equivalent crack opening at the onset of softening and the maximum equivalent crack opening. These parameters may be chosen such that, for a given fracture strength σ_c, fracture toughness G_c and an initial cohesive stiffness K,

$$\Delta_i = \frac{\sigma_c}{K}\,, \qquad \Delta_f = \frac{2G_c}{\sigma_c}\,,$$

where the initially linearly "elastic" loading up to the fracture strength in a bi-linear law can be reproduced in (4) by assigning an initial damage $\kappa(0) = \kappa_0 = \Delta_i$. The parameters Δ_i and Δ_f are chosen such that the maximum of the function $\hat{T}$ in (4) equals the fracture strength σ_c and the integral of $\hat{T}$ from $\Delta = 0$ to $\Delta = \Delta_f$ equals the material fracture energy (toughness) G_c.

After evaluating (4), the normal and shear tractions can be computed as

$$t_n = \begin{cases} \dfrac{\delta_n}{\Delta} T & \text{if} \quad \delta_n > 0, \\ K\delta_n & \text{if} \quad \delta_n < 0, \end{cases} \tag{6}$$

$$t_s = \gamma^2 \frac{\delta_s}{\Delta} T\,,$$

i.e., for $\delta_n \ge 0$, one has that $\boldsymbol{t} \cdot \boldsymbol{\delta} = T\Delta$.

2.2. Crack healing model

The cohesive relation summarized in the previous section can be extended to formulate a cohesive crack-healing model. The single healing case is discussed first, which is then followed by a generalized model capable of multiple healing events.

2.2.1. Single healing event

The proposed crack healing model is a composite-based constitutive model for simulating the recovery of fracture properties upon activation of crack healing. The traction components of the composite response, $\tilde{t}_n$ and $\tilde{t}_s$, are expressed as a weighted sum of the traction contributions from the original material, $t_n^{(0)}$ and $t_s^{(0)}$, and the healing material $t_n^{(1)}$ and $t_s^{(1)}$, as follows:

$$\tilde{t}_n = w^{(0)} t_n^{(0)} + w^{(1)} t_n^{(1)} \qquad \tilde{t}_s = w^{(0)} t_s^{(0)} + w^{(1)} t_s^{(1)} \tag{7}$$

where the superscripts (0) and (1) represent the original and healing materials, respectively. The weighting factors $w^{(0)}$ and $w^{(1)}$ introduced in (7), which can take values between 0 and 1, are the primary parameters in the model and can be interpreted as the surface-based volume fractions of the original and healing material respectively at the instance of healing activation. The meaning of "volume fraction" in this context refers to the fraction of the crack area occupied by a material per unit crack opening displacement. In a two-dimensional setting, the crack area fraction refers to the crack length fraction per unit depth. As indicated in (7), it is assumed that a partially damaged area that has been healed contains contributions from both the original material and the healing material. Correspondingly, the weighting factors $w^{(0)}$ and $w^{(1)}$ are related to fractions of a partially damaged surface where the original material is still capable of transmitting a force (in the sense of a cohesive relation) while the healing material has occupied the complementary region. Observe that this assumption implies that the model is essentially based on an "equal strain" distribution among the phases (Voigt model), in this case with the crack opening playing the role of a strain-like variable. Consequently, the tractions in each phase may be overpredicted compared to a model based on an "equal stress" assumption (Reuss model), however the current Voigt-like model preserves kinematic compatibility whereas a Reuss-like model does not.

In order to develop the constitutive model, define an energy-based damage parameter $D^{(0)}$ as follows:

$$D^{(0)}(t) := \frac{G_d^{(0)}(t)}{G_c^{(0)}} \tag{8}$$

which represents the ratio between the energy dissipated $G_d^{(0)}(t)$ during decohesion of the original material up to time t and the fracture energy $G_c^{(0)}$ (work required for complete decohesion of the original material). In a bilinear cohesive relation, as presented in Section 2.1, this parameter may be approximated as

$$D^{(0)}(t) \approx \frac{\kappa^{(0)}(t)}{\Delta_f^{(0)}}$$

where the initial, undamaged "elastic" response has been neglected (namely it is assumed in (5) that $\Delta_f^{(0)} \gg \Delta_i^{(0)}$).

Prior to healing, the cohesive response is characterized by the cohesive relation of the original material, i.e., with $w^{(1)} = 0$ in (7). If a single healing event occurs at a time $t = t^*$, the proposed constitutive model assumes that the factor $w^{(1)}$ is given by the value of the energy-based damage parameter at the instance of healing activation, $D^{(0)*}$, i.e.,

$$w^{(1)} = D^{(0)^*} := \frac{G_d^{(0)^*}}{G_c^{(0)}} \ . \tag{9}$$

Correspondingly, a value $w^{(1)} = 0$ upon healing activation represents zero equivalent damaged area fraction of the original material at a given material point (i.e., the original material is fully intact) while $w^{(1)} = 1$ represents a fully-damaged original material at a given material point (i.e., the healing material would occupy the fully damaged material point upon healing). The interpretation of (9) is that the volume fraction $w^{(1)}$ available for the healing material in order to fill and heal can be determined from the value of the energy-based damage parameter of the original material, defined in (8) at the instance of the healing activation. Upon healing of the available volume fraction $w^{(1)}$, the volume fraction of the original material, $w^{(0)}$, assumes a value equal to $1 - w^{(1)}$, which is equal to the equivalent undamaged area of the original material. Conversely, the energy-based damage parameter can be interpreted as an equivalent damaged area fraction at a given material point in the context of the cohesive zone framework. A schematic of the traction–separation relations for a material point under damage and healing is shown in Fig. 2 depicting the features of the model.

In accordance with (7) and (9), the effective fracture energy $\tilde{G}_c$ of the composite material after healing becomes the weighted sum of the fracture energies of the original and healing materials, given as

$$\tilde{G}_c = w^{(0)} G_c^{(0)} + w^{(1)} G_c^{(1)} \ . \tag{10}$$

2.2.2. Traction-crack opening relations: original material

The traction–separation relation corresponding to the original material *after healing* is governed by a modified effective displacement-based cohesive crack model explained as follows: the effective displacement for the original material defined in the conventional cohesive zone model is modified by introducing shifts in normal and tangential crack opening displacements to take into account the effect of healing. These shifts in the crack opening displacements lead to a modified effective displacement for the original material, $\Delta^{(0)}$, given as

$$\Delta^{(0)} := \sqrt{\left\langle \delta_n - \delta_n^{(0)^*} \right\rangle^2 + \gamma^2 (\delta_s - \delta_s^{(0)^*})^2}, \quad t \geq t^* \ . \tag{11}$$

The reason for introducing the shift is as follows: on activation of a healing process, the healing agent diffuses/flows through the crack and crack filling occurs thereby (fully or partially) reducing the crack opening. As a result, the crack opening displacements after complete healing should be considered nominally zero. To simulate this process, displacement shifts are introduced into the crack opening displacements, which make the nominal opening displacement zero upon complete healing. Further, a shift is also applied in the crack opening history variable, κ, which is reset to its initial value. This is done to simulate the intact portion of the original material point, whereas the damaged portion of the considered material point is assumed to be healed by the healing material.

In a cohesive-zone model, a partially-damaged material has a non-zero crack opening displacement but it may still be capable of transmitting a force. In the present model, if healing is activated in a partially damaged surface, it is assumed that the process occurs at constant stress provided there is no change in the external loading.

The shifts introduced in the normal and the tangential crack opening displacements for the original material are given as follows:

$$\begin{aligned} \delta_n^{(0)*} &= \delta_n^* - t_n^*/(w^{(0)} K) \ , \\ \delta_s^{(0)*} &= \delta_s^* - t_s^*/(w^{(0)} K) \ . \end{aligned} \tag{12}$$

In the above expressions, δ_n^* and δ_s^* are the actual crack opening displacements in the original material at the instant of crack

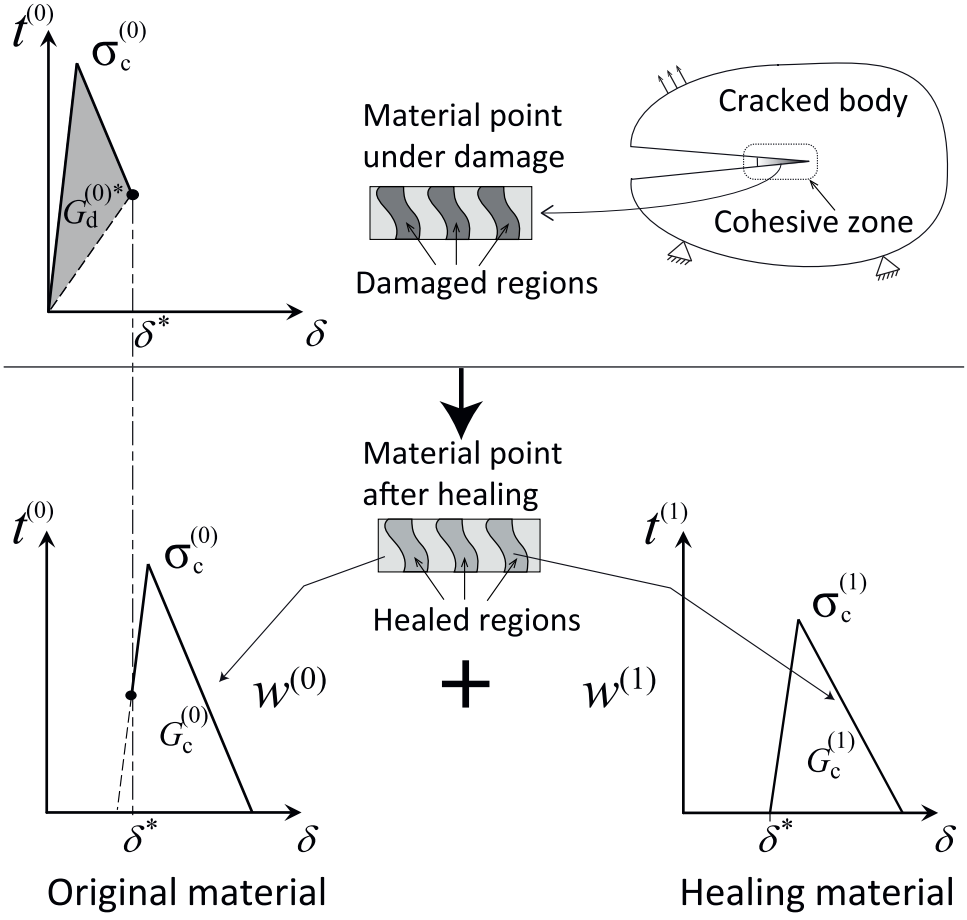

Fig. 2. Traction–separation laws of original and healing material, which upon weighted addition, results in a composite cohesive relation for the crack-healing model.

healing activation. As shifts in crack opening displacements are introduced along with restoration of the crack opening history variable κ, the shifts in crack opening displacements are constructed in such a way that the tractions across the cohesive surface maintain their continuity. Consequently, the traction components t_n^* and t_s^* across the partially damaged surface remain the same before and after healing activation.

The normal and shear tractions corresponding to the original material during subsequent loading after healing are then obtained from the corresponding traction–separation relations (4) and (6) using the aforementioned equivalent opening $\Delta^{(0)}$, i.e.,

$$t_n^{(0)} = \begin{cases} \dfrac{(\delta_n - \delta_n^{(0)^*})}{\Delta^{(0)}} T(0) & \text{if} \quad \delta_n > \delta_n^{(0)*}, \\ K(\delta_n - \delta_n^{(0)^*}) & \text{if} \quad \delta_n < \delta_n^{(0)*}, \end{cases} \tag{13}$$

$$t_s^{(0)} = \gamma^2 \frac{(\delta_s - \delta_s^{(0)^*})}{\Delta^{(0)}} T(0).$$

2.2.3. Traction-crack opening relations: healing material

Similar to the original material, the traction–separation relations corresponding to the healing material are governed by a modified equivalent displacement variable, $\Delta^{(1)}$ defined as

$$\Delta^{(1)} := \sqrt{\left\langle \delta_n - \delta_n^{(1)^*} \right\rangle^2 + \gamma^2 (\delta_s - \delta_s^{(1)^*})^2}, \tag{14}$$

where $\delta_n^{(1)^*}$ and $\delta_s^{(1)^*}$ are shifts applied to the traction–separation relation of the healing material. The shifts are introduced into the crack opening displacements of the healing material following the same approach as for the original material. The main difference is that the healing material is assumed to transmit zero load at the instant of healing activation. Thus, the shifts in crack opening displacements for the healing material are the actual crack opening displacements at the instant of healing activation, i.e.,

$$\begin{aligned} \delta_n^{(1)*} &= \delta_n^* \\ \delta_s^{(1)*} &= \delta_s^*. \end{aligned} \tag{15}$$

Similar to the approach adopted for the original material after healing, the normal and tangential traction components corresponding to the healing material are obtained from an equivalent traction $T^{(1)}$ of the corresponding traction–separation relations (4) and (6) using the equivalent opening $\Delta^{(1)}$, i.e.,

$$t_n^{(1)} = \begin{cases} \dfrac{(\delta_n - \delta_n^{(1)^*})}{\Delta^{(1)}} T(1) & \text{if} \quad \delta_n > \delta_n^{(1)*}, \\ K(\delta_n - \delta_n^{(1)*}) & \text{if} \quad \delta_n < \delta_n^{(1)*}, \end{cases} \tag{16}$$

$$t_s^{(1)} = \gamma^2 \frac{(\delta_s - \delta_s^{(1)*})}{\Delta^{(1)}} T^{(1)}.$$

It is worth noticing that, in both the original and healing material phases, the shifts in the crack opening displacements are applied at the component level, i.e., individually on the normal and tangential components. The composite tractions $\tilde{t}_n$ and $\tilde{t}_s$, given in (7), are obtained through a rule-of-mixtures approach analogous to an equal strain assumption used for composite materials (in this case an equal crack opening assumption) with material-specific responses given by (13) and (16). This approach provides sufficient

flexibility to specify separate material properties and fracture behavior for the original and healing materials.

2.2.4. Multiple healing events

The approach presented in the previous section can be extended to account for multiple healing events. This generalization is capable of dealing with a complex history of (partial) crackings and healings. In the sequel, the index p refers to the number of healing events, ranging from 0 to m, with the convention that $p = 0$ represents the undamaged original state. The index p may also be used to represent the healing material phase that is formed during the pth healing event, again with the convention that $p = 0$ corresponds to the original material. At the end of the mth healing event, the composite-like traction components $\tilde{t}_{\mathrm{n}}^{[m]}$ and $\tilde{t}_{\mathrm{s}}^{[m]}$ of the multiply-healed material are given by

$$\tilde{t}_{\mathrm{n}}^{[m]} = \sum_{p=0}^{m} w^{[m](p)} t_{\mathrm{n}}^{(p)} \qquad \tilde{t}_{\mathrm{s}}^{[m]} = \sum_{p=0}^{m} w^{[m](p)} t_{\mathrm{s}}^{(p)} \tag{17}$$

where $t_{\mathrm{n}}^{(p)}$ and $t_{\mathrm{s}}^{(p)}$ are the normal and tangential traction components of the pth material phase and $w^{[m](p)}$ is the volume fraction of the pth material phase (index in parentheses) present or created at the mth healing event (index in square brackets). The relation given in (17) is a generalization of (7) for the case $m > 1$. For modeling purposes, a separate index is assigned to each new healing material created at the pth healing event even though the actual materials (chemical composition) may be physically the same. The purpose is to keep track of their individual evolutions throughout a complex loading and healing process starting at possibly different states (i.e., every healing instance is recorded separately). In accordance with the proposed constitutive model for the single healing event, it is assumed that the volume fraction $w^{[m](p)}$ of the pth material phase is related to the energy-based damage parameter of that phase prior to the mth healing event, which can be expressed recursively as

$$w^{[m](p)} = \begin{cases} 1 & \text{for } p = m = 0, \\ w^{[m-1](p)}\left(1 - D^{[m](p)}\right) & \text{for } 1 \le p < m\ , \\ \sum_{p=0}^{m-1} w^{[m-1](p)} D^{[m](p)} & \text{for } 1 \le p = m\ . \end{cases} \tag{18}$$

In the above expression, $D^{[m](p)}$ is the value of energy-based damage parameter $D^{(p)}$ corresponding to the pth healing phase at the mth healing event. With this notation, the term $D^{(0)^*}$ in (9) can alternatively be expressed as $D^{[1](0)}$ to indicate the value of the energy-based damage parameter evaluated at the instant at which the first healing event is activated. It is also to be noted that the sum of all $w^{[m](p)}$ is equal to 1, where p ranges from 0 to m.

The fracture energy $\tilde{G}_{\mathrm{c}}^{[m]}$ of a multiply-healed composite-like crack, which is a generalization of (10) for $m > 1$, corresponds to the weighted sum of the fracture energies of the phases $p = 0, \ldots, m-1$ available before healing activation and the fracture energy of the latest formed healing material $p = m$, i.e.,

$$\tilde{G}_{\mathrm{c}}^{[m]} = \sum_{p=0}^{m} w^{[m](p)} G_{\mathrm{c}}^{(p)}\ . \tag{19}$$

At the mth healing event, there are $m+1$ material phases at a material point within the cohesive zone for which the tractions in each phase are governed by the corresponding cohesive relations. The shifts in the crack opening displacements are obtained for each phase such that the continuity of the tractions is maintained within each phase, similar to the equations for the shifts given by (12) and (15).

For subsequent use, the expressions for the volume fractions $w^{[m](p)}$ in the case of two healing events are obtained explicitly from (18) with $m = 2$, i.e.,

$$\begin{aligned} w^{[2](0)} &= w^{[1](0)}\left(1 - D^{[2](0)}\right) = \left(1 - D^{[1](0)}\right)\left(1 - D^{[2](0)}\right)\ , \\ w^{[2](1)} &= w^{[1](1)}\left(1 - D^{[2](1)}\right) = D^{[1](0)}\left(1 - D^{[2](1)}\right)\ , \\ w^{[2](2)} &= w^{[1](0)} D^{[2](0)} + w^{[1](1)} D^{[2](1)} \\ &= \left(1 - D^{[1](0)}\right) D^{[2](0)} + D^{[1](0)} D^{[2](1)}\ . \end{aligned} \tag{20}$$

The damage in the original material up to the first healing event is reflected in the value $D^{[1](0)}$ whereas the subsequent damage in the original material and the first healing material is accounted for, respectively, through the values $D^{[2](0)}$ and $D^{[2](1)}$. The corresponding composite traction and fracture energy after the second healing event can be computed from (17) and (19).

2.3. Numerical implementation

The cohesive crack healing model described above can be implemented in a finite element framework using cohesive elements (or using an XFEM approach). In the context of a finite element solution procedure performed using a Newton–Raphson iterative approach, the contribution of the cohesive elements to the global stiffness matrix is provided by their element-wise consistent tangent matrix, which corresponds to the derivative of the traction vector with respect to the crack opening displacement. With respect to a local coordinate system normal (n) and tangential (s) to the crack, the components of the tangent matrix are, in view of (17), given by the weighted constitutive (material) tangents of each phase p, i.e.,

$$\frac{\partial \tilde{t}_i^{[m]}}{\partial \delta_j} = \sum_{p=0}^{m} w^{[m](p)} \frac{\partial t_i^{(\mathrm{p})}}{\partial \delta_j}\ , \quad i = \mathrm{n},\ \mathrm{s}, \quad j = \mathrm{n},\ \mathrm{s}\ . \tag{21}$$

Correspondingly, the tangent matrix of the composite-like model requires the individual contributions from the phases. The expressions for the constitutive stiffness tangents depend on the loading–unloading conditions, as indicated in (3), applied separately for each phase p.

Under softening condition:

For $f^{(p)} = 0$ and $\dot{\kappa}^{(p)} > 0$, the components of the consistent tangent matrix for the phase p are obtained, assuming that $\Delta_{\mathrm{i}}^{(p)} \ll \Delta_{\mathrm{f}}^{(p)}$, from (4), (5), (11) and (13), as follows:

$$\begin{aligned} \frac{\partial t_{\mathrm{n}}^{(p)}}{\partial \delta_{\mathrm{n}}} &= \sigma_{\mathrm{c}}^{(p)} \left[\frac{1}{\Delta^{(p)}} - \frac{1}{\Delta_{\mathrm{f}}^{(p)}} - \frac{\left\langle \delta_{\mathrm{n}} - \delta_{\mathrm{n}}^{(p)*} \right\rangle^2}{(\Delta^{(p)})^3} \right]\ , \\ \frac{\partial t_{\mathrm{s}}^{(p)}}{\partial \delta_{\mathrm{s}}} &= \gamma^2 \sigma_{\mathrm{c}}^{(p)} \left[\frac{1}{\Delta^{(p)}} - \frac{1}{\Delta_{\mathrm{f}}^{(p)}} - \frac{\gamma^2 \left(\delta_{\mathrm{s}} - \delta_{\mathrm{s}}^{(p)*}\right)^2}{(\Delta^{(p)})^3} \right]\ , \\ \frac{\partial t_{\mathrm{n}}^{(p)}}{\partial \delta_{\mathrm{s}}} &= \frac{\partial t_{\mathrm{s}}^{(p)}}{\partial \delta_{\mathrm{n}}} = -\frac{\gamma^2 \sigma_{\mathrm{c}}^{(p)} \left\langle \delta_{\mathrm{n}} - \delta_{\mathrm{n}}^{(p)*} \right\rangle \left(\delta_{\mathrm{s}} - \delta_{\mathrm{s}}^{(p)*}\right)}{(\Delta^{(p)})^3}\ . \end{aligned}$$

Under unloading/reloading conditions:

For $f^{(p)} < 0$ and $\dot{\kappa}^{(p)} = 0$, the components of the consistent tangent matrix are, assuming that $\Delta_{\mathrm{i}}^{(p)} \ll \Delta_{\mathrm{f}}^{(p)}$, given as

$$\begin{aligned} \frac{\partial t_{\mathrm{n}}^{(p)}}{\partial \delta_{\mathrm{n}}} &= \sigma_{\mathrm{c}}^{(p)} \left[\frac{1}{\kappa^{(p)}} - \frac{1}{\Delta_{\mathrm{f}}^{(p)}} \right]\ , \\ \frac{\partial t_{\mathrm{s}}^{(p)}}{\partial \delta_{\mathrm{s}}} &= \gamma^2 \sigma_{\mathrm{c}}^{(p)} \left[\frac{1}{\kappa^{(p)}} - \frac{1}{\Delta_{\mathrm{f}}^{(p)}} \right]\ , \\ \frac{\partial t_{\mathrm{n}}^{(p)}}{\partial \delta_{\mathrm{s}}} &= \frac{\partial t_{\mathrm{s}}^{(p)}}{\partial \delta_{\mathrm{n}}} = 0\ . \end{aligned}$$

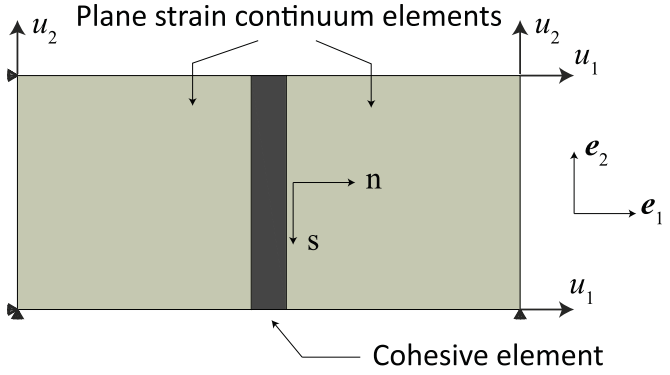

Fig. 3. Three element model: an initially zero thickness cohesive element placed in between two continuum two dimensional plane strain elements.

The case of the initial "elastic" behavior can in principle be treated formally as a reloading case by assigning an initial damage $\kappa_0^{(p)} = \Delta_i^{(p)}$. However, since in the previous formulas the term $\Delta_i^{(p)}$ has been neglected, the tangent matrix can be separately specified as

$$\frac{\partial t_n^{(p)}}{\partial \delta_n} = \frac{1}{\gamma^2}\frac{\partial t_s^{(p)}}{\partial \delta_s} = K \ ,$$

$$\frac{\partial t_n^{(p)}}{\partial \delta_s} = \frac{\partial t_s^{(p)}}{\partial \delta_n} = 0 \ ,$$

where K is the cohesive stiffness, assumed in this case to be the same for all phases.

3. Model evaluation and testing

In this section, the model is tested using a simple three-element mesh as shown in Fig. 3, in which a single zero-thickness cohesive element is placed between two continuum elements of size $20\,\mu m \times 20\,\mu m$ each. Several aspects are considered to study the behavior of the model, which include different loading conditions, number of healing events, properties of the healing material and the degree of damage.

3.1. Fracture and healing in monotonic straining

In the first set of test simulations, the three-element system is subjected to various monotonic straining conditions to study the behavior of the cohesive element under damage and healing. The loading conditions are prescribed through applied displacements as shown in Fig. 3. The time history of the specified displacement is shown in Fig. 4a, which corresponds to a three-stage deformation, namely (i) a nominally mode-I opening stage involving a linear increase in applied deformation, (ii) a rest period with healing at the maximum deformation reached in the first stage and (iii) a resumption of the mode-I deformation. In all the simulations, it is assumed that complete healing occurs at the end of the zero loading-rate time period (rest period). The post-healing behavior of the cohesive element corresponds to the third stage. For the present model, the actual duration of the rest period has no direct effect on the simulations since the healing kinetics are not modeled explicitly; only the state of the healing material upon resumption of the loading is relevant. However, the healing period is indicated in the time history for clarity and to emphasize that healing is, in general, a process with time scales comparable to (and sometimes larger than) the time scales associated to mechanical loading.

For the conditions assumed in the simulation, the evolution of the stress in the cohesive zone in a three-element system only depends on the fracture properties but not on the elastic properties of the bulk material. The fracture properties of the original and healing materials are given as

$$\sigma_c^{(0)} = 100\,\text{MPa}, \quad \sigma_c^{(1)} = 75, 100\,\text{MPa}, \quad \Delta_f^{(0)} = \Delta_f^{(1)} = 2\,\mu m.$$

As indicated above, two values are considered regarding the fracture strength $\sigma_c^{(1)}$ of the healing material, namely a lower strength compared to the original material (chosen as 75% of $\sigma_c^{(0)}$) and an equal strength (100%). The healing materials and the original material have the same final crack opening Δ_f. In principle, it is possible to consider the case of a healing material that has a higher strength, but in order to study that situation, it is more relevant to carry out an analysis with more than one cohesive element where a secondary crack is allowed to initiate elsewhere.

The effective traction as a function of time is shown in Fig. 4b for both values of the fracture strength of the healing material. As shown in the figure, the traction in the cohesive element initially increases up to the value equal to cohesive strength $\sigma_c^{(0)}$ of the original material and then decreases as a result of damage evolution. Complete failure occurs when the crack opening reaches the critical crack opening for failure $\Delta_f^{(0)}$ of the original phase. Afterwards, the crack opening continues to grow due to the externally-imposed deformation at essentially zero stress. As indicated in Fig. 4a, healing is activated at $t = 100$ s (and is assumed to be completed at $t = 300$ s). Correspondingly, a shift in the crack opening of $\delta_n^{(1)*} = 3\,\mu m$ and $\delta_s^{(1)*} = 0$ is taken into account and the loading is resumed. The maximum load is reached at the corresponding value of the fracture strength of the healing material $\sigma_c^{(1)}$ for both cases considered (75% and 100%). The loading continues in the softening (degradation) regime until the healing material completely fails, which occurs when the shifted crack opening is such that $\Delta^{(1)} = \Delta_f^{(1)}$.

The effect of the damage due to loading and the recovery due to healing can be seen in Fig. 4c in terms of the relevant damage variables as a function of time. During the first stage of loading, the damage variable $D^{(0)}$ of the original material increases from 0 to 1, which indicates that the original material undergoes full damage. The healing process in the second stage is not modeled explicitly but rather provided as input for the cohesive model to analyze the recovery of strength. During that process, the damage variable $D^{(0)}$ of the original material remains at 1 while the damage variable $D^{(1)}$ of the healing material becomes active with an initial value equal to zero (no damage). During the third stage of the process, the damage variable $D^{(1)}$ of the healing material increases from 0 to 1, hence at the end of the loading process the healing material is also fully damaged.

The results of the simulation can also be reported in terms of the traction across the cohesive interface as a function of the crack opening displacement as shown in Fig. 4d. Although the loading process in this example is relatively simple, it illustrates the importance of using the shift in the crack opening variable to properly simulate the evolution of stress during healing. Indeed, as may be observed in Fig. 4d, the material follows the expected cohesive response starting from the value $\Delta^{(1)} = 3\,\mu m$ as a new origin after healing.

3.2. Multiple healing of a partially-damaged material

The next example to illustrate the features of the model pertains to multiple healing of a partially-damaged material. In this case, the material is loaded and healed according to the applied deformation shown in Fig. 5a. As indicated in the figure, the material is initially extended and undergoes partial damage. Subsequently, the material is healed and the loading is resumed, which generates partial damage of the original and the healing material. The material then experiences a second healing event before

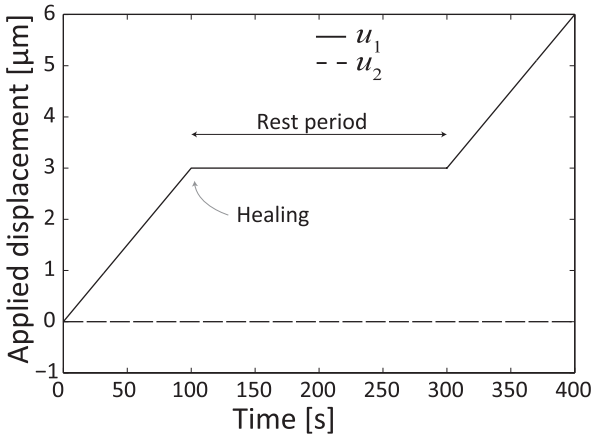

(a) Specified displacement-time history.

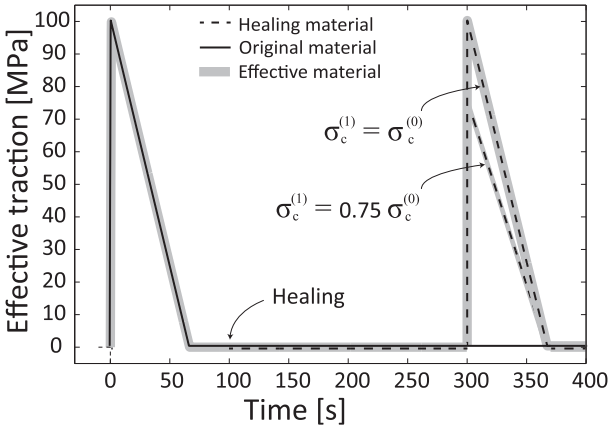

(b) Traction history in the cohesive element

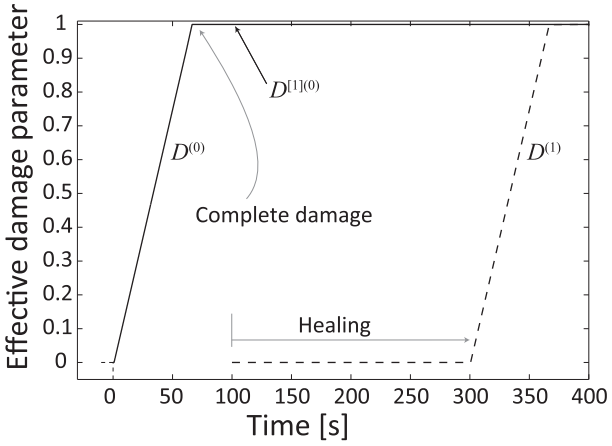

(c) Time history of damage in the cohesive element

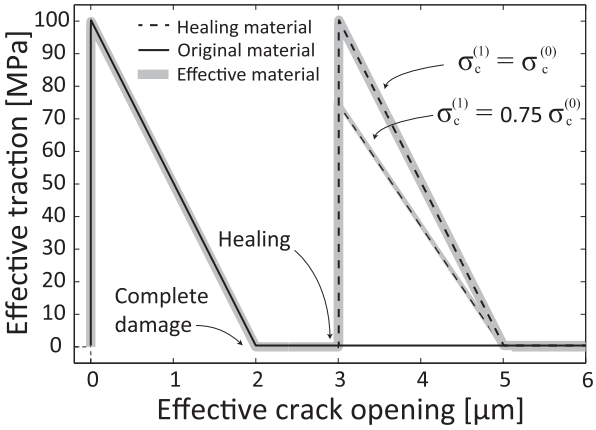

(d) Traction vs. crack opening in the cohesive element

Fig. 4. Case 1: Illustration of response of cohesive element under monotonic straining, healing and further straining. The response includes the cases of healing materials with fracture strengths equal 75% and 100% of the strength of the original material.

loading is resumed until final failure. In this simulation, the fracture strength of the healing materials are chosen as $\sigma_c^{(1)} = \sigma_c^{(2)} = 0.75\sigma_c^{(0)}$ with the actual values as indicated in the previous subsection.

The evolution of the effective (composite) normal traction $\tilde{t}_n^{[m]}$ and the phase-weighted tractions $w^{[m](p)}t_n^{(p)}$ are shown in Fig. 5b as a function of time. The effect of healing on the fracture strength is reflected in the distinct peak values of the response. The first peak corresponds to the fracture strength $\sigma_c^{(0)}$ of the original material. The second peak lies between the one of the original material and the healed material since the original material was not fully damaged before healing was activated, hence it partly contributes to the effective (composite) fracture strength. In that case the strength is $w^{[1](0)}t_n^{(0)} + w^{[1](1)}\sigma_c^{(1)}$, with $t_n^{(0)}$ being the stress on the original material at the instant that the stress on the first healing material reaches its critical value. Similarly, the third peak contains contributions from the three phases that are active at that instant, namely it is given by $w^{[2](0)}t_n^{(0)} + w^{[2](1)}t_n^{(1)} + w^{[2](2)}\sigma_c^{(2)}$, with $t_n^{(0)}$ and $t_n^{(1)}$ being the stresses on the original and first healing material at the instant that the stress on the second healing material reaches its critical value.

The evolution of the damage parameter for each phase is shown in Fig. 5c, where it can be seen that the rate of damage per phase decreases as the number of active phases increases (i.e., the damage gets distributed among the different phases, with the largest rate corresponding to the most recently created phase). The effective traction–separation relation for multiple healing of a partially-damaged material is shown in Fig. 5d. The effective fracture energy, as given by (19), depends on the number of healing events and the volume fractions $w^{[m](p)}$. As may be inferred from Fig. 5d, the total fracture energy of the material, measured as the area under the curve, increases as a result of the healing process compared to the original material.

3.3. Unloading after healing of partially-damaged material

In order to validate the unloading features of the cohesive model, the three-element system is subjected to a loading and healing process as indicated in Fig. 6a. In this case the material is extended, undergoes partial damage followed by healing, after which extension is resumed and finally the material is unloaded. The unloading is specified in terms of displacement, which ends at the displacement for which the stress vanishes. The fracture

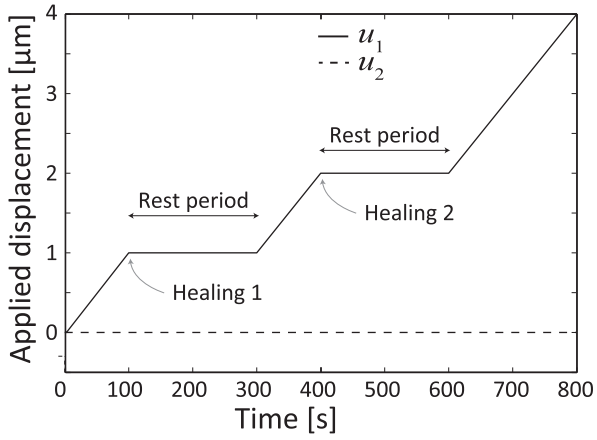

(a) Specified displacement-time history.

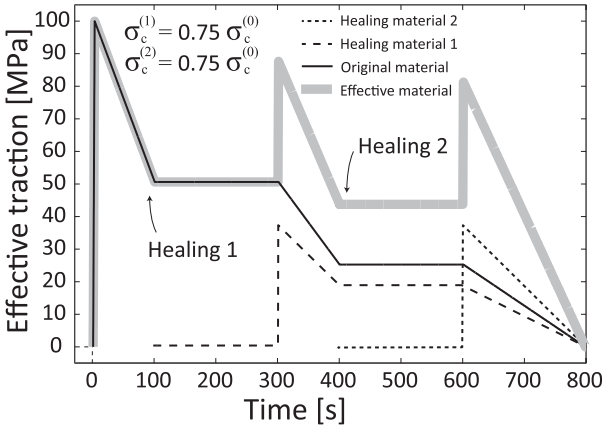

(b) Traction history in the cohesive element

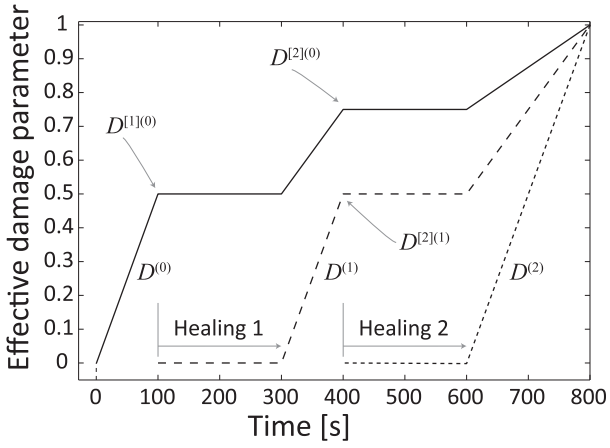

(c) Time history of damage in the cohesive element

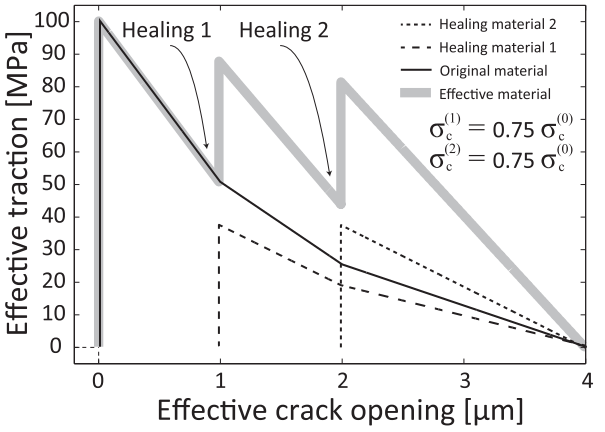

(d) Traction vs. crack opening in the cohesive element

Fig. 5. Case 2: Illustration of response of cohesive element considering partial damage and healing. The fracture strength of the healing material is assumed to be equal to 75% of that of the original material.

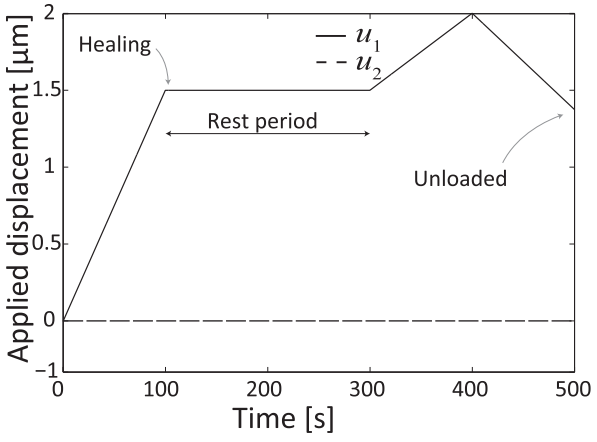

(a) Specified displacement-time history.

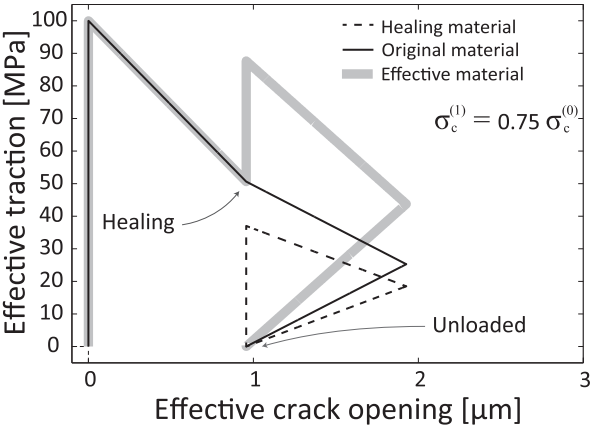

(b) Traction vs. crack opening displacement

Fig. 6. Case 3: Partial damage, healing, partial damage and unloading. The fracture strength of the healing material is assumed to be equal to 75% of that of the original material.

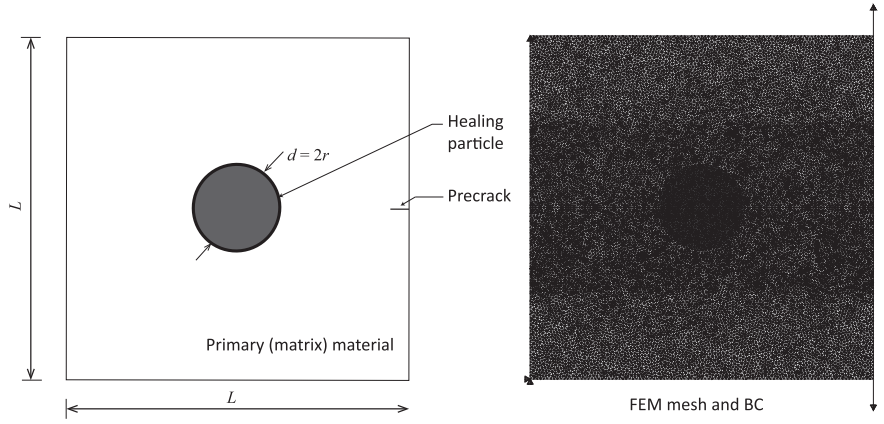

Fig. 7. Geometry and finite element model of a unit cell of an extrinsic self-healing material. The unit cell is subjected to a nominal mode I loading. A small precrack is used to guide a matrix crack towards the particle. A layer of cohesive elements is placed to allow for crack propagation in a predefined direction given by the initial precrack.

strength of the healing material is taken as $\sigma_c^{(1)} = 0.75\sigma_c^{(0)}$. The effective traction as a function of crack opening is shown in Fig. 6b. As may be observed in the figure, upon unloading, the stress returns elastically to zero along the corresponding unloading curve of each phase, which depends on the damage parameter of the specific phase. The stress is zero at the crack opening displacement at which healing occurred according to the shift parameters given in (12) and (15).

Other loading cases, not shown here for conciseness, indicate that the model is able to predict the behavior under complex sequences of mixed-mode loading, unloading and healing. The application of the healing cohesive model under non-homogeneous conditions is analyzed in the following section.

4. Application to particle-based extrinsic self-healing material

In this section, the cohesive healing model is applied to a unit cell of an extrinsic self-healing material in which a single healing particle is embedded within a matrix material as shown in Fig. 7. In extrinsic systems, the particle contains a healing agent (i.e., the material contained inside the particle) that is normally protected by an encapsulation system to prevent premature activation of the healing process. The working principle of this system is that the healing mechanism is activated when a crack that propagates through the matrix interacts with the particle, usually breaking the encapsulation and allowing transport of the healing agent through the crack. Some self-healing system may involve auxiliary materials that are necessary for triggering and/or participating in a subsequent chemical reaction to create the final form of the healing material. The present simulation assumes that any additional substance required for the process is readily available in the matrix material (e.g., free oxygen transported by diffusion required for oxidation as found in self-healing thermal barrier coatings Sloof et al., 2015). Distinct cohesive relations can be used at different spatial locations (matrix, particle, matrix–particle interface), hence phase-specific fracture properties can be specified for the healing agent inside the particle and the healing material that appears in the cracks after activation of the healing mechanism.

As shown in Fig. 7, the unit cell used in the simulations is an $L \times L$ domain with a circular particle of a diameter $d = 2r$. For simplicity a two-dimensional computational domain under plane strain conditions is chosen, meaning that the particle should be interpreted as prismatic (fiber in the out-of-plane direction). Despite this interpretation, the model is assumed to be qualitatively representative of a spherical particle albeit with a different volume fraction. In the simulations, the length is chosen as $L = 75\,\mu\text{m}$ and the diameter as $d = 10\,\mu\text{m}$, which corresponds to a nominal (in-plane) particle volume fraction of 14%. In the finite element mesh, cohesive elements are inserted along a horizontal plane in the mid-height of the model, by which the crack is allowed to propagate along the pre-defined path. In principle, arbitrary crack growth can be modeled by inserting cohesive elements along all bulk elements in mesh, although that approach is not required for purposes of the present study (Ponnusami et al., 2015b). The finite element mesh is sufficiently resolved so that proper discretization of the cohesive zone is ensured. Displacement-driven nominal mode I load is applied by specifying vertical displacements at the corner nodes on the right side of the domain while the corner nodes at the left are fixed as shown in the figure. Both the matrix and the healing particle are assumed to be isotropic and linearly elastic up to fracture. For the sake of simplicity, the material properties (both elastic and fracture) of the matrix and the healing particle are kept the same and the values are given as follows:

$$E^{\text{m}} = E^{\text{p}} = 150\,\text{GPa}, \quad \nu^{\text{m}} = \nu^{\text{p}} = 0.25,$$
$$\sigma_c^{\text{m}} = \sigma_c^{\text{p}} = \sigma_c^{(0)} = 400\,\text{MPa}, \quad G_c^{\text{m}} = G_c^{\text{p}} = G_c^{(0)} = 100\,\text{J/m}^2,$$

where E and ν refer to Young's modulus and Poisson's ratio, respectively, and the superscripts m and p refer to the matrix and the particle, respectively. Since the properties of the particle and the matrix are assumed to be equal, the original material, as indicated by the superscript 0, refers to either the particle or the matrix depending on location. The interface between the particle and the matrix is assumed to be perfectly bonded and interface fracture is taken not to occur. It is worth pointing out that in general the elastic and fracture properties of the healing particle and the matrix are different, which in fact decide whether a matrix crack would break the healing particle or not. This aspect of a matrix crack interacting with healing particles of different properties compared to the matrix is dealt in detail in Ponnusami et al. (2015b) but is not relevant for the simulations presented in this section. Instead, emphasis is placed here on how the crack healing behavior affects the recovery of mechanical properties of the material system. Further, as indicated above, the fracture properties of the healing particle in its initial state are in general different than the properties of the healing material that fills the cracks, which are specified separately as explained in the sequel.

Several parametric studies are conducted to evaluate the behavior of the unit cell and the results in terms of global load-displacement response are reported in the following subsections. In the first subsection, simulations are conducted to study the effect of variations in the fracture properties of the healing material. In the second subsection, a parametric study is performed to

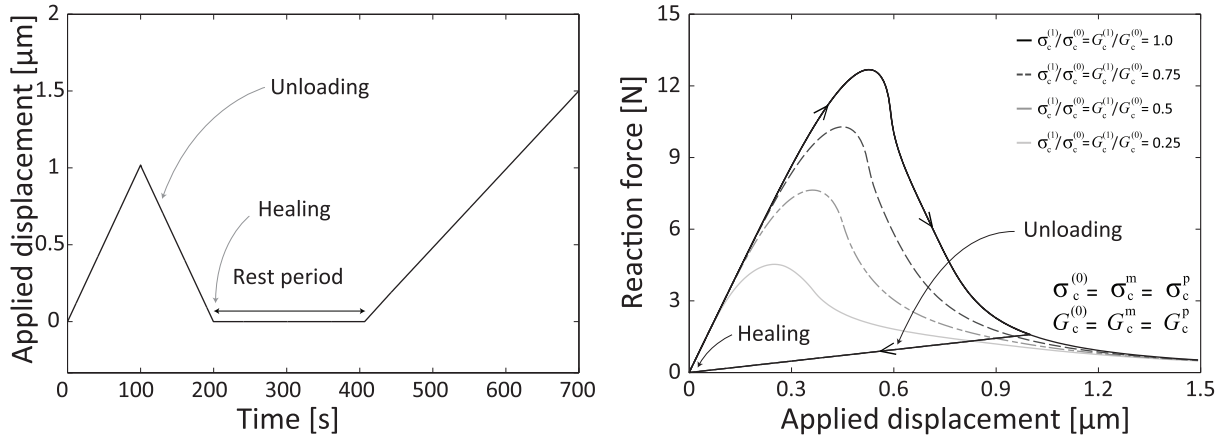

(a) Time history of the specified displacement. (b) Reaction force vs. applied displacement

Fig. 8. Healing under unloaded condition: applied loading to unit cell and reaction force as a function of applied displacement for various values of the fracture properties of the healed material.

understand how does the available amount of healing agent affect the crack healing behavior. In the third subsection, multiple healing events are simulated and the resulting load-displacement response is reported.

4.1. Effect of properties of healing material and healing conditions

The fracture properties of the healing material, formed as the result of the healing process, are often different from the surrounding host material. The fracture properties of the healed zone depend on the time available for healing and the properties of the healing product. A second aspect that is relevant for the healing process is the loading conditions during healing. Healing is a process that typically requires time to occur, and the efficiency of the process is often connected to providing a sufficiently long "rest time" in which the loading rate is zero and chemical reactions have sufficient time to be completed. However, even if a sufficient "rest time" is provided, the (constant) loading state influences the subsequent material response of the healed material. In this section, two representative loading states during healing are considered, namely healing under zero-stress (unloaded) conditions and healing under fixed applied displacement (constant load during healing). Different properties for the healing material are considered for each loading state during healing.

4.1.1. Healing under unloaded condition

In the literature, most experimental studies deal with test protocols in which the sample is unloaded and allowed to return to its unstrained state, hence healing occurs under unloaded conditions (Kessler et al., 2003; Brown et al., 2002; Williams et al., 2007; Pang and Bond, 2005b; Song et al., 2008). In order to analyze the predictions of the model under similar conditions, the unit cell shown in Fig. 7 is subjected to a loading and healing sequence as indicated in Fig. 8a. Under this loading, the specimen is partially fractured and then unloaded. Healing is allowed to occur in the unloaded condition, which is then followed by reloading of the healed specimen. The response of the unit cell in terms of the applied vertical displacement and the corresponding reaction force is shown in Fig. 8b for various fracture properties of the healing material, namely $\sigma_c^{(1)}/\sigma_c^{(0)}$, $G_c^{(1)}/G_c^{(0)} = 0.25$, 0.5, 0.75 and 1, where the superscript 1 refers to the healing material. As shown in Fig. 8b, the curve corresponding to equal properties of the healing and original material predicts a recovery of the response after healing similar to that of the original material. The next three curves correspond to lower values of the fracture properties of the healing material and hence the load-displacement curves fall below that of the original material after healing.

It is to be mentioned that, after healing, recracking occurs along the same path as the initial crack. This is due to the fact the fracture properties of the healing material are lower than or at least equal to that of the original material properties. Nonetheless, if the properties of the healing material are higher than that of the original material, the crack would propagate along a different path which is weaker than the healed zone. However, the recovered load-displacement response would be similar to the one with the same fracture properties, as the crack is traversing along the original material.

4.1.2. Healing under constant load condition

In situations of practical interest, healing may occur under a non-zero load, which implies that the crack opening is non-zero as the healing material fills the crack gap. To study the effect of the loading state during healing on the post-healing response of the material, simulations are carried out according to the loading sequence shown in Fig. 9a. In this case, the specimen is (partially) fractured, allowed to heal at a constant applied displacement and subsequently reloaded. As in the previous case (healing at unloaded conditions), four different fracture properties of the healing material are considered, given by the strength and fracture energy ratios $\sigma_c^{(1)}/\sigma_c^{(0)}$, $G_c^{(1)}/G_c^{(0)} = 0.25$, 0.5, 0.75 and 1. The load carrying capability of the healed specimens is shown in Fig. 9b, which indicates the reaction force of the unit cell as a function of the applied vertical displacement.

For each set of material properties of the healing material, the state of the specimen is the same prior to healing. After healing at a constant crack opening profile, the specimen recovers its load-carrying capability as shown in Fig. 9a. It can be observed that the post-healing force peak is higher than the force peak of the original material for the case when the healing material has the same fracture properties of the original material. This result is partly due to the equal strain kinematic assumption of the Voigt-like composite model, as indicated in Section 2.2.1, which tends to overpredict the force response. It is anticipated that a more complex composite model, which preserves both linear momentum and kinematic compatibility, would predict a lower post-healing peak. Although the present model provides an upper estimate of the post-healed behavior, it allows to compare the effect of the state of the material during healing on the post-healing behavior. In particular, the

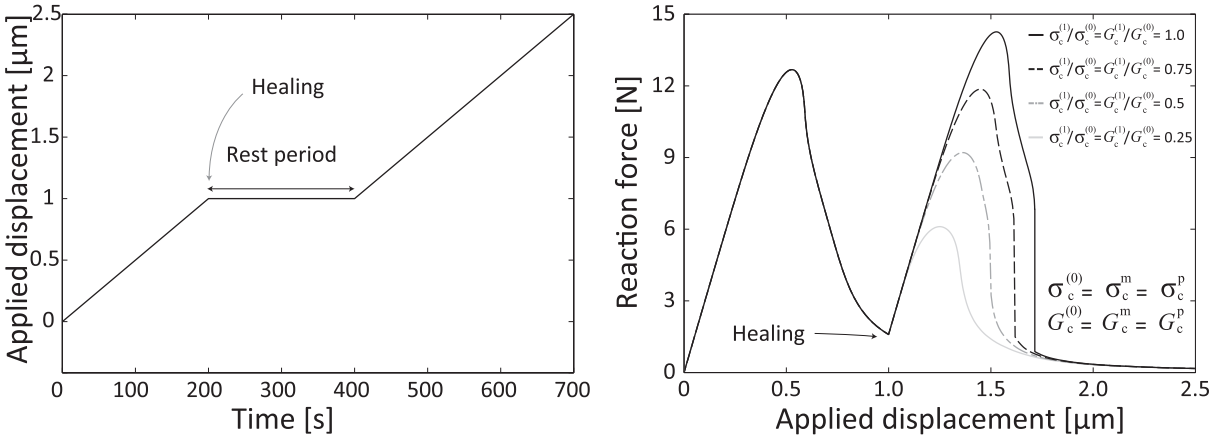

(a) Time history of the specified displacement. (b) Reaction force vs. applied displacement

Fig. 9. Healing under constant loading condition: applied loading to unit cell and reaction force as a function of applied displacement for various values of the fracture properties of the healed material.

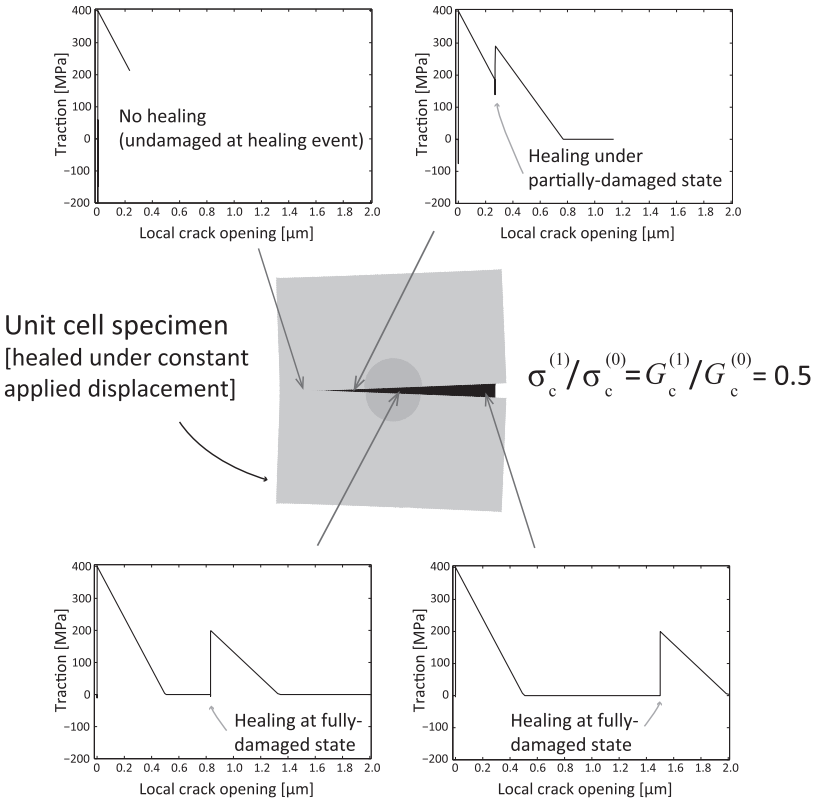

Fig. 10. Unit cell specimen at the final state of the applied loading given in Fig. 9a. Representative local response curves illustrate how the introduction of a shift in the (local) crack opening displacement accounts for the proper origin upon resumption of the load after healing.

post-healing failure in the case of healing under loaded conditions is more sudden (i.e., qualitatively more brittle, see Fig. 9b) compared to the case of healing at an unloaded state (see Fig. 9b), except when the properties of the healing material are relatively low.

To gain more insight in the healing process under constant crack opening profile, the local response curves at selected locations are shown in Fig. 10 for the case when the properties of the healing material are $\sigma_c^{(1)}/\sigma_c^{(0)} = G_c^{(1)}/G_c^{(0)} = 0.5$. As can be observed in the figure, the crack openings at the instant of healing depend on location, with increasing values towards the side where the opening load is applied. Observe that some points undergo healing from a fully-failed state, some from a partially-failed state and some points that are cracked at the end of the loading process experienced no healing since they had not failed at the instant at which healing was activated.

After healing, the effective crack opening displacements become zero in the healed zone due to the displacement shifts introduced in the model to account for crack filling. However, modeling of the crack gap filling and healing is only done implicitly through the shift in crack opening displacements, whereby the new material is not explicitly modeled as an additional material (or mass) entering the system.

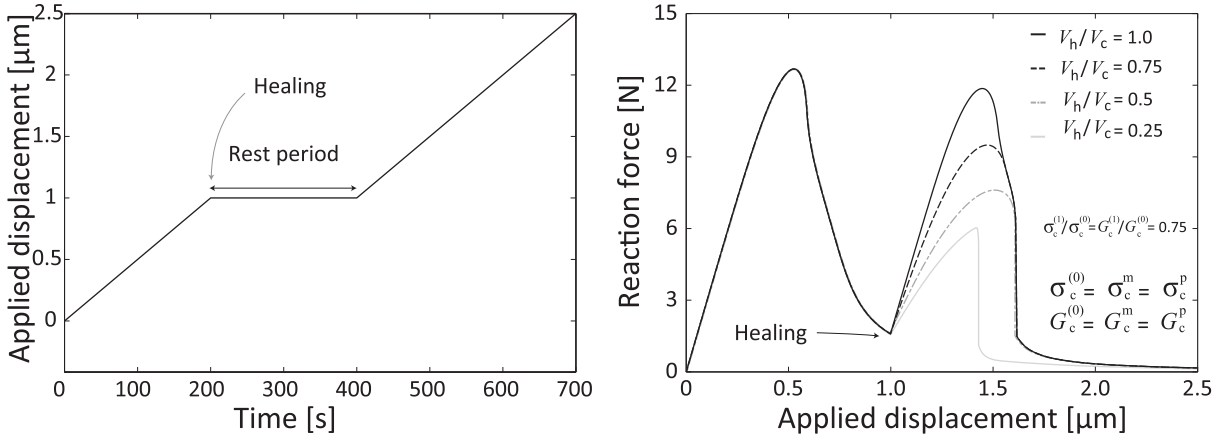

(a) Time history of the specified displacement. (b) Reaction for vs. applied displacement

Fig. 11. Effect of filling efficiency: applied loading to unit cell and reaction force as a function of applied displacement for various values of healed areas.

4.2. Degree of crack filling and healing

In the previous subsection, it was assumed that the healing particle, upon fracture, releases an amount of healing agent (denoted as V_h) that is sufficient for complete filling of the crack opening volume (or crack opening area in two dimension, denoted as V_c). However, depending on the amount of available healing material, the geometrical characteristics of the crack and the mode of transport, it may occur that the crack is only partially filled, which is a key factor affecting the healing characteristics and hence the recovery of mechanical properties. In this section, the effect of the ratio V_h/V_c of healing agent available to the required healing agent for complete filling is studied. Here, the volume of required healing agent for complete crack filling refers to the total crack volume at the instance of healing activation. The ratio considered is generic and its interpretation in a specific self-healing material system requires understanding of its healing characteristics. For instance, the amount of healing material produced as the result of the healing process is directly related not only to the volume of the healing particle, but also the reaction kinetics of the healing process. For example, in one of the extrinsic self-healing systems reported in the literature, the healing agent within the particle produces healing material through increase in volume by oxidation under high temperature conditions (Sloof et al., 2015; Ponnusami et al., 2015a). Hence, the term V_h means here the volume of the healing product formed as the result of the healing process, which is used for healing the crack. The notion of complete or partial filling, measured by the ration V_h/V_c, refers to the amount of crack gap filled with healing material regardless of the fracture properties of the healing material.

Simulations are conducted for four different healing processes with filling efficiencies of $V_h/V_c = 1$, 0.75, 0.5 and 0.25. In all cases the properties of the healing material are taken as $\sigma_c^{(1)}/\sigma_c^{(0)}$, $G_c^{(1)}/G_c^{(0)} = 0.75$. The specimens are loaded according to the sequence indicated in Fig. 11a and the corresponding force–displacement curves are shown in Fig. 11b. To interpret the results for partial filling, it is useful to indicate the spatial location where healing occurs, which is shown in Fig. 12. As indicated in the figure, filling is assumed to take place in the zone adjacent to the healing particle.

The curve shown in Fig. 11b corresponding to a complete filling (filling ratio $V_h/V_c = 1$) represents the highest possible recovery of the load-carrying capability for the given fracture properties of the healing material. As expected, the recovery of the load-carrying capability decreases with decreasing filling ratios $V_h/V_c = 0.75, 0.5, 0.25$. One relevant difference between the effect of a decrease in filling efficiency and a decrease in the fracture properties of the healing material for a fixed filling efficiency is that in the latter case the initial slope of the post-healed behavior remains the same for distinct fracture properties whereas in the former case the initial slope decreases with decreasing filling efficiency (compare Figs. 9b and 11b). In the simulations shown in Fig. 11b, the initial post-healing slope reflects the increase in compliance due to purely geometrical effects. The un-healed portion of the crack facilitates the (elastic) deformation of the specimen. This effect may potentially be used in the interpretation of experimental curves as an indication of partial filling of a crack.

4.3. Multiple healing events

Some materials with intrinsic self-healing capacity (such as MAX phases), may undergo multiple healing events whereby a crack is healed on multiple occasions (Li et al., 2012; Sloof et al., 2016). In extrinsic systems, multiple healing may occur in cases where there is an external supply of healing material, but also in particle-based systems when inactivated particles (or portions of partially activated particles) can still supply healing material for an additional healing event. In this section, it is assumed that the particle in the unit cell shown in Fig. 7 is capable of providing sufficient healing material for two healing events. The specimen is subjected to a loading and healing process as shown in Fig. 13a. The ratio of crack opening volume (or area) to the available healing material volume is assumed to be 1 for both healing events, resulting in complete filling of the crack. The fracture properties of the healing material after the first healing event are taken as 75% of those of the original material, while for the second healing event, the properties are taken as 50% of that of the original material, hence $\sigma_c^{(1)}/\sigma_c^{(0)}$, $G_c^{(1)}/G_c^{(0)} = 0.75$ and $\sigma_c^{(2)}/\sigma_c^{(0)}$, $G_c^{(2)}/G_c^{(0)} = 0.5$. This assumption is meant to implicitly represent a degradation on the quality of the healing material after the first healing event.

The reaction force on the unit cell is shown in Fig. 13b as a function of the applied vertical displacement. As can be observed in the figure, the load carrying capacity may be (partially) recovered multiple times provided that the self-healing mechanism supplies sufficient healing material for multiple healing events. Although a single healing event can naturally extend the lifetime of a material, a more significant extension can be achieved in a material capable of multiple self-healing repairs, even if the quality of the healing material degrades during subsequent healing events.

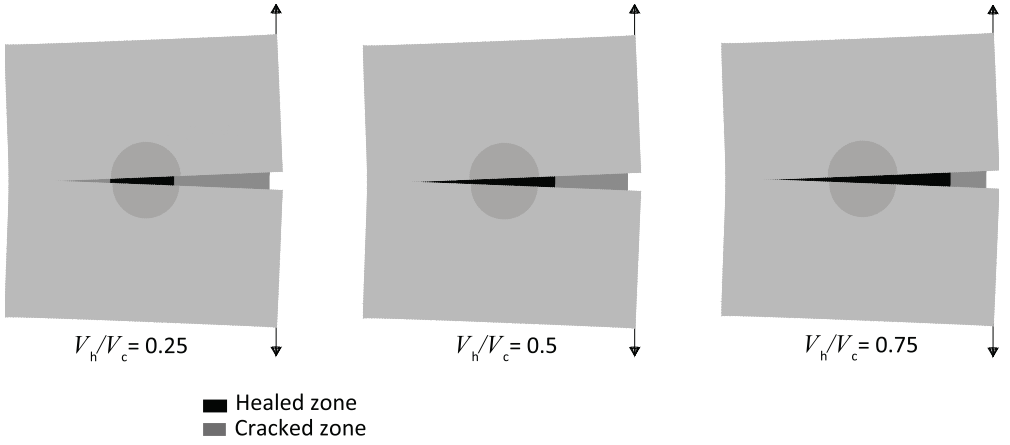

Fig. 12. Specimen showing the healed cohesive cracks for various degrees of crack filling. For the purpose of clarity, the deformed specimen has a scaling factor of 3.

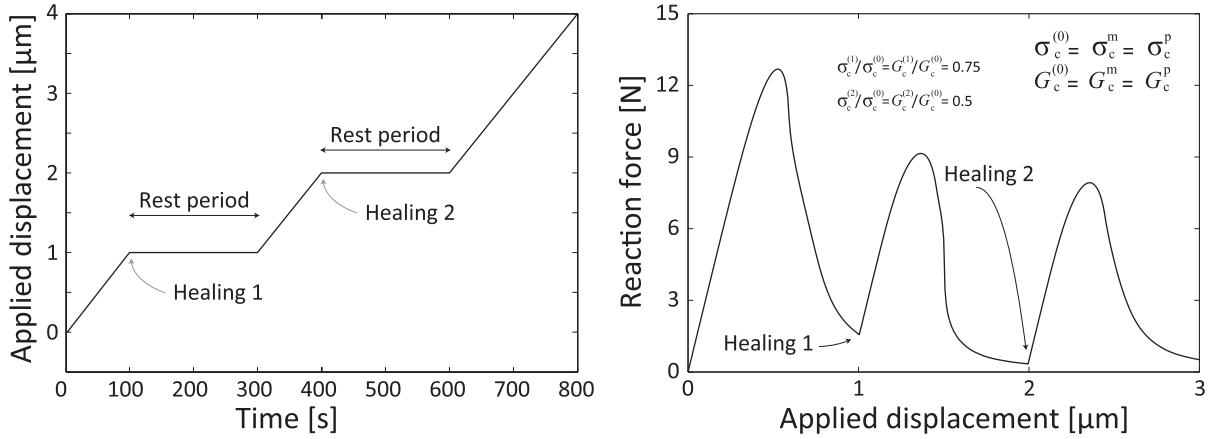

(a) Time history of the specified displacement. (b) Reaction for vs. applied displacement

Fig. 13. Effect of multiple healing: applied loading to unit cell and reaction force as a function of applied displacement for two healing events.

The model developed here may be used for design purposes to optimize the characteristics of a healing particle and/or a cluster of healing particles by further investigating convenient particle characteristics or particle arrangements that provide the capacity of multiple healing events. This may be achieved by, for example, embedding particles large enough to serve as a reservoir for multiple healing events or by placing a cluster of particles that may be activated sequentially as cracks re-appear in a material at adjacent locations. Although those studies are beyond the scope of the current work, the present model may be employed to simulate the recovery of strength and fracture energy under complex loading histories.

5. Summary and outlook

A cohesive zone-based computational framework for analyzing self-healing materials is presented to model the recovery of mechanical properties. Salient features of the composite model are demonstrated through several test simulations. In particular, the capability of the model to simulate multiple healing events and handling different fracture properties of the healing material for each healing event is relevant for analyzing several realistic self-healing materials. The model can be applied for either extrinsic or intrinsic self-healing material systems with an appropriate coupling to healing kinetics in each case.

For a unit cell of an extrinsic self-healing material, the simulations show that the recovery of the load carrying capacity upon healing depends both on the fracture properties of the healing material that fills the cracks as well as the filling efficiency, which may be seen as a geometrical characteristic. Further, it is found that the post-healed behavior of a material healed under loaded conditions appears to be more brittle than for a material healed under unloaded conditions, although this conclusion is based on the assumption that the healing material has the same fracture properties in both cases, which may not be necessarily the case in some self-healing materials. The simulations also indicate that the characteristics of the initial post-healing response in a force-displacement diagram may be used as an indicator of the filling efficiency of a healing event whereby an initial response similar to that of the original material corresponds to maximum crack filling efficiency regardless of the fracture properties of the healing material. A decrease in the initial post-healing force-displacement slope compared to the initial slope of the original material is an indication of an incomplete filling process, again regardless of the fracture properties of the healing material.

The developed framework does not explicitly model the crack healing kinetics, rather the results of the healing process are provided as input parameters to the model. Nonetheless, the coupling of crack healing kinetics into the model is in principle straightforward in the form of the amount of healing material produced as the result of the healing process, which is then geometrically re-

lated to the crack volume healed. For modeling purposes, it is also possible to treat the properties of the healing material as a variable during multiple healing events to implicitly account for a continuous degradation in the healing quality. In general, the model may be used for designing new self-healing material systems with the capacity of undergoing multiple healing events and, correspondingly, extending significantly the lifetime of a material with minimal external intervention.

Acknowledgments

This work was funded in part by IOP Self Healing Materials (Agentschap NL, now Rijksdienst voor Ondernemend Nederland RVO) through Project SHM01021 and in part by the European Union's Seventh Framework Program (FP7) through the NMP SAMBA project (Grant number 309849). We thank the IOP Self-Healing Materials and the Seventh European Framework Programme for their financial support of our research. We extend our sincere thanks to our collaborator Prof. W.G. Sloof for his valuable support and interactive discussions.

References

Alsheghri, A.A., Al-Rub, R.K.A., 2015. Thermodynamic-based cohesive zone healing model for self-healing materials. Mech. Res. Commun. 70, 102–113.
Barbero, E.J., Greco, F., Lonetti, P., 2005. Continuum damage–healing mechanics with application to self-healing composites. Int. J. Damage Mech. 14 (1), 51–81.
Bergman, S.D., Wudl, F., 2008. Mendable polymers. J. Mater. Chem. 18 (1), 41–62.
Blaiszik, B., Kramer, S., Olugebefola, S., Moore, J.S., Sottos, N.R., White, S.R., 2010. Self-healing polymers and composites. Annu. Rev. Mater. Res. 40, 179–211.
Bluhm, J., Specht, S., Schröder, J., 2015. Modeling of self-healing effects in polymeric composites. Arch. Appl. Mech. 85 (9–10), 1469–1481.
Brown, E.N., Sottos, N.R., White, S.R., 2002. Fracture testing of a self-healing polymer composite. Exp. Mech. 42 (4), 372–379.
Carabat, A.L., van der Zwaag, S., Sloof, W.G., 2015. Creating a protective shell for reactive $MoSi_2$ particles in high-temperature ceramics. J. Am. Ceram. Soc. 98 (8), 2609–2616.
Darabi, M.K., Al-Rub, R.K.A., Little, D.N., 2012. A continuum damage mechanics framework for modeling micro-damage healing. Int. J. Solids Struct. 49 (3), 492–513.
Dry, C., 1994. Matrix cracking repair and filling using active and passive modes for smart timed release of chemicals from fibers into cement matrices. Smart Mater. Struct. 3 (2), 118.
Gilabert, F., Garoz, D., Van Paepegem, W., 2017. Macro- and micro-modeling of crack propagation in encapsulation-based self-healing materials: application of XFEM and cohesive surface techniques. Mater. Des. 130, 459–478.
Herbst, O., Luding, S., 2008. Modeling particulate self-healing materials and application to uni-axial compression. Int. J. Fract. 154 (1–2), 87–103.
Kessler, M., Sottos, N., White, S., 2003. Self-healing structural composite materials. Compos. A: Appl. Sci. Manuf. 34 (8), 743–753.
Li, S., Song, G., Kwakernaak, K., van der Zwaag, S., Sloof, W.G., 2012. Multiple crack healing of a Ti_2AlC ceramic. J Eur Ceram Soc 32 (8), 1813–1820.
Luding, S., Suiker, A.S., 2008. Self-healing of damaged particulate materials through sintering. Philos. Mag. 88 (28–29), 3445–3457.
Maiti, S., Geubelle, P.H., 2006. Cohesive modeling of fatigue crack retardation in polymers: crack closure effect. Eng. Fract. Mech. 73 (1), 22–41.
Mergheim, J., Steinmann, P., 2013. Phenomenological modelling of self-healing polymers based on integrated healing agents. Comput. Mech. 52 (3), 681–692.
Ozaki, S., Osada, T., Nakao, W., 2016. Finite element analysis of the damage and healing behavior of self-healing ceramic materials. Int. J. Solids Struct. 100, 307–318.
Pang, J., Bond, I., 2005a. 'Bleeding composites'—damage detection and self-repair using a biomimetic approach. Compos. A: Appl. Sci. Manuf. 36 (2), 183–188.
Pang, J.W., Bond, I.P., 2005b. A hollow fibre reinforced polymer composite encompassing self-healing and enhanced damage visibility. Compos. Sci. Technol. 65 (11), 1791–1799.
Ponnusami, S., Turteltaub, S., Zhang, X., Xiao, P., 2015a. Modelling crack propagation in particle-dispersed self-healing thermal barrier coatings. In: van der Zwaag, S., Brinkman, E. (Eds.), Self healing materials – Pioneering research in The Netherlands. IOS Press, Netherlands, pp. 229–241.
Ponnusami, S.A., Turteltaub, S., van der Zwaag, S., 2015b. Cohesive-zone modelling of crack nucleation and propagation in particulate composites. Eng. Fract. Mech. 149, 170–190.
Šavija, B., Feiteira, J., Araújo, M., Chatrabhuti, S., Raquez, J.-M., Van Tittelboom, K., Gruyaert, E., De Belie, N., Schlangen, E., 2016. Simulation-aided design of tubular polymeric capsules for self-healing concrete. Materials 10 (1), 10.
Schimmel, E., Remmers, J., 2006. Development of a constitutive model for self-healing materials. Technical report. Delft Aerospace Computational Science.
Sloof, W., Turteltaub, S., Derelioglu, Z., Ponnusami, S., Song, G., 2015. Crack healing in yttria stabilized zirconia thermal barrier coatings. In: van der Zwaag, S., Brinkman, E. (Eds.), Self healing materials – Pioneering research in The Netherlands. IOS Press, Netherlands, pp. 219–227.
Sloof, W.G., Pei, R., McDonald, S.A., Fife, J.L., Shen, L., Boatemaa, L., Farle, A.-S., Yan, K., Zhang, X., van der Zwaag, S., et al., 2016. Repeated crack healing in MAX-phase ceramics revealed by 4D in situ synchrotron X-ray tomographic microscopy. Sci. Rep. 6, Article Number 23040.
Song, G., Pei, Y., Sloof, W., Li, S., De Hosson, J.T.M., Van der Zwaag, S., 2008. Oxidation-induced crack healing in Ti_3AlC_2 ceramics. Scr. Mater. 58 (1), 13–16.
Toohey, K.S., Sottos, N.R., Lewis, J.A., Moore, J.S., White, S.R., 2007. Self-healing materials with microvascular networks. Nat. Mater. 6 (8), 581–585.
Ural, A., Krishnan, V.R., Papoulia, K.D., 2009. A cohesive zone model for fatigue crack growth allowing for crack retardation. Int. J. Solids Struct. 46 (11), 2453–2462.
Van Tittelboom, K., De Belie, N., 2013. Self-healing in cementitious materials—a review. Materials 6 (6), 2182–2217.
Voyiadjis, G.Z., Shojaei, A., Li, G., 2011. A thermodynamic consistent damage and healing model for self healing materials. Int. J. Plast. 27 (7), 1025–1044.
Voyiadjis, G.Z., Shojaei, A., Li, G., Kattan, P.I., 2012. A theory of anisotropic healing and damage mechanics of materials. Proc. R. Soc. Lond. A: Math. Phys. Eng. Sci 468 (2137), 163–183.
White, S.R., Sottos, N., Geubelle, P., Moore, J., Kessler, M., Sriram, S., Brown, E., Viswanathan, S., 2001. Autonomic healing of polymer composites. Nature 409 (6822), 794–797.
Wiktor, V., Jonkers, H.M., 2011. Quantification of crack-healing in novel bacteria-based self-healing concrete. Cem. Concr. Compos. 33 (7), 763–770.
Williams, G., Trask, R., Bond, I., 2007. A self-healing carbon fibre reinforced polymer for aerospace applications. Compos. A: Appl. Sci. Manuf. 38 (6), 1525–1532.
Xu, W., Sun, X., Koeppel, B.J., Zbib, H.M., 2014. A continuum thermo-inelastic model for damage and healing in self-healing glass materials. Int. J. Plast. 62, 1–16.
Zemskov, S.V., Jonkers, H.M., Vermolen, F.J., 2011. Two analytical models for the probability characteristics of a crack hitting encapsulated particles: application to self-healing materials. Comput. Mater. Sci 50 (12), 3323–3333.
van der Zwaag, S., 2008. Self healing materials: an alternative approach to 20 centuries of materials science. Springer Science + Business Media BV.